13th Spring School on Transition and Turbulence
September 19th-23rd, 2022, Blumenau, SC, Brazil

EPTT-2022-0026
PARTICLE FRAGMENTATION IN TURBULENT DENSE GAS-SOLID FLUIDIZED BEDS JETS: FRAGMENTATION POTENTIAL MODELING, PARAMETRIC SENSITIVITY ANALYSIS AND CFD-BASED OPTIMIZATION

Richard Tribess
Otto-von-Guericke-Universität Magdeburg, Faculty of Process and Systems Engineering, MPS, Hoher Weg 7b, 06120 Halle (Saale)
richard.tribess@ovgu.de

Celso Murilo dos Santos
Regional University of Blumenau, Chemical Engineering Department, Rua São Paulo 3250, 89030-000, Blumenau
celsomurilo@furb.br

Waldir Pedro Martignoni
Regional University of Blumenau, Chemical Engineering Department, Rua São Paulo 3250, 89030-000, Blumenau
wmartignoni@gmail.com

Dirceu Noriler
State University of Campinas, Faculty of Chemical Engineering, Av. Albert Einstein, 500, 13083-852, Campinas
dnoriler@unicamp.br

Henry França Meier
Regional University of Blumenau, Chemical Engineering Department, Rua São Paulo 3250, 89030-000, Blumenau
meier@furb.br

Abstract. *The gas distributor region of dense gas-solid fluidized beds is characterized by enhanced momentum rates and high solids concentration gradients. The high gas injection velocities can potentialize unwanted effects such as the bed material attrition, which can become a problem, affecting the fluidization process efficiency due to drastic changes in the particulate material properties. The design parameters of the injection nozzles found in gas distributors systems play a serious role in the particulate material fragmentation. This study aims at describing a fragmentation potential, considering the relationship between the breakage probability and the collision frequency between two particles, in a Euler-Euler framework using the TFM-KTGF model. 2D-axisymmetric simulations are performed and the influence of the injection nozzle design parameters is evaluated through a parametric sensitivity study. Based on the significant variables obtained from the parametric sensitivity study, the fragmentation potential is employed as an objective function to be minimized in a CFD-based optimization using the COMPLEX algorithm. Through the performed analysis, it was possible to observe that the proposed fragmentation potential is highly influenced by the injection nozzle's design parameters, mainly the orifice diameter and the tube diameter, with differences of up to 600 times between the analyzed test cases. Smaller orifice diameters and bigger tube diameters showed considerably smaller results for the fragmentation potential. This behavior is related to smaller mean velocities in the nozzle outlet and larger orifice-to-particle diameter ratios. During the optimization procedure, a tendency for the inlet nozzles to reach the same geometrical characteristics was observed, according to the geometrical restrictions employed.*

Keywords: *Dense Fluidized Beds, Attrition, Computational Fluid Dynamics, Parametric Sensitivity Analysis, CFD-Based Optimization*

1. INTRODUCTION

Fluidized beds are employed in many industrial processes, such as coating, granulation, drying, and the synthesis of fuels and base chemicals. Different flow regimes are observed in fluidized beds according to the solid phase volume fraction and the gas superficial velocity (Lim *et al*., 1995), as well as the particulate material properties, identified via the Geldart classification (Geldart, 1973). In conventional dense fluidized beds, the bubbling, slugging and turbulent flow regimes are found, depending on the region observed. Bubbling and slugging regimes are predominant in the grid zone

while the turbulent regime mainly occurs in the gas injection region. The gas injection is made through the use of perforated plates or pipe grids, designed to obtain a homogeneous distribution on the cross-section of the fluidized bed (Sadeghbeigi, 2020). The injection of high velocity gas through orifices or nozzles can lead to the formation of jets, which are characterized by enhanced momentum, heat and mass transfer rates, as well as substantial concentration gradients (Sauriol *et al*., 2013). Jets play a key role regarding the fluidization as a whole, however, the high velocity impact between particles accelerated by the gas jet and those with lower momentum located in the dense bed can induce a harmful effect: the particulate material kinetic attrition.

The kinetic attrition of particulate material can severely modify the particle size distribution and consequently important fluidization characteristics of the bed, affecting the equipment performance. This effect can be classified according to mechanisms that occur at different energy levels: abrasion and fragmentation (Vaux and Keairns, 1980). Abrasion happens in the dense region of the fluidized bed, on which bubbles or slugs are responsible for the gas-solid interactions. Particle-particle contact happens with low impact velocities; therefore, abrasion is known as a low energy mechanism. The high energy mechanism is known as fragmentation and takes place in the high momentum rates and concentration gradient regions, on which high impact velocity particle-particle collisions occur, such as the jets region (Yang, 2003). Several empirical correlations were developed to model the abrasion and fragmentation mechanisms for different operational conditions, particulate materials, and gas injection systems, such as orifices and nozzles (McMillan *et al*., 2007; Zhang *et al*., 2016). However, empirical correlations can only be used for the conditions employed during their development. In this sense, the use of a phenomenological approach can be an interesting alternative when the extrapolation of operational conditions and injection nozzle design parameters is necessary (Grace *et al*., 2020).

With the increase in computational power during the last decades, the mathematical tool Computational Fluid Dynamics (CFD) has been employed in many studies regarding multiphase flows. Different approaches employing Eulerian-Eulerian or Eulerian-Lagrangian frameworks are available for modeling the behavior of gas-solid flows in fluidized beds. The appropriate approach must be chosen according to the analyzed system scale, such as the domain size and the amount of particulate material present therein, as well as the relation between the computational effort and the precision required for the flow description (Van der Hoef *et al*., 2008).

The TFM-KTGF model is commonly employed in the description of engineering scale gas-solid flows. In this Eulerian-Eulerian approach, the gas and solid phases are treated as continuum and interpenetrating through the use of the Navier Stokes Equations combined with the Kinetic Theory of Granular Flows (Gidaspow, 1994). The CFD-DEM model employs a Eulerian-Lagrangian framework on which a continuum approach is adopted for the gas phase description and the solid phase is considered discrete, described through Newton's law considering *soft-sphere* or *hard-sphere* approaches (Van de Hoef *et al*., 2008). The use of appropriate models for the interphase momentum exchange plays a mandatory role in the flow description, as well as consistent boundary conditions (Chalermsinsuwan *et al*., 2011).

Pougatch *et al.* (2010) proposed a particle fragmentation model for the jet's region based on a TFM-KTGF approach relating the granular temperature with mechanical properties of the particulate material. They evaluated the breakage efficiency in a *coking* process and the obtained good agreement with experimental data. Zhang *et al*. (2014) studied the behavior of a dense fluidized bed composed of magnetite particles and derived a collision frequency model based on a TFM-KTGF approach. Fulchini *et al*. (2017) and Ghods *et al*. (2019) employed a CFD-DEM approach to describe the behavior of the jet's region of dense fluidized beds. Fulchini *et al*. (2017) employed Ghadiri and Zhang's (2002) fragmentation model to account for the particle size distribution variation and validated their simulations with Scirocco's standardized experimental test. Ghods *et al*. (2019) proposed two particle-breakage models based on the contact forces determined through a *soft-sphere* model and in the Weibull breakage probability function, also accounting for the particle size distribution variation. The CFD-DEM approach directly accounts for particle-particle collisions and contact forces, and the description of particle breakage can be easily accessed. However, its use is limited for dozens of thousands of particles, which is not the case for dense fluidized beds on engineering scale. Therefore, the TFM-KTGF model is more suitable for the study of these systems.

Through the use of a consistent CFD model, aligned with a proper description for the studied effect, it is possible to propose modifications regarding operational conditions and/or design parameters aiming at minimizing or maximizing a variable of interest through optimization procedures. The surface response methodology was employed by Wu *et al*. (2019) and Kang *et al*. (2020) for the optimization of dense fluidized beds employing the TFM-KTGF model to obtain data for the proposed analysis. However, this methodology results are only applicable for the range of operational conditions or design parameters employed on their development, being used to obtain the best possible configuration of variables for the effect minimization or maximization. This methodology is not suitable for obtaining a global optimal condition (Saario *et al*., 2006). Optimization procedures based on the minimization or maximization of an objective function through the use of mathematical models or algorithms such as the COBYLA (Powell, 2007) and the Nelder-Mead algorithm, also known as COMPLEX (Nelder and Mead, 1965; Box, 1965) is suitable for the search of the global optimal conditions. Sgrott Jr *et al*. (2015) employed the COMPLEX algorithm on the multi-objective optimization of cyclones, maximizing the collect efficiency and minimizing the pressure drop. Luciano *et al*. (2018) employed the COBYLA algorithm on the multi-objective optimization of multi-cyclone systems.

In many industrial processes, the fragmentation of the particulate material is a serious problem and must be avoided. The present work aims at the proposal of a particle fragmentation model based on a Eulerian-Eulerian TFM-KTGF

approach, described as a function of the breakage probability from Pougatch *et al*. (2010) and the collision frequency proposed by Zhang *et al*. (2014). The influence of the design parameters the gas inlet nozzle on the fragmentation potential is studied through a statistical Parametric Sensitivity Analysis via the *p-value* analysis. The inlet nozzle orifice diameter (d_{or}), tube diameter (d_t), orifice thickness (h_{or}), tube height (h_t) and tube wall thickness (w_t) are employed in a 2^5 factorial experimental design, with the lower limit and upper limit based on a standard inlet nozzle geometry employed in the Electrical Capacitance Tomography Experimental Unit (LP-ECT) operated in the Regional University of Blumenau (FURB), considering values 13% below and above the standard test case, respectively. The significant variables obtained through the Parametric Sensitivity Analysis are employed as manipulated variables in a CFD-Based optimization through the use of the COMPLEX algorithm with the objective of minimizing the fragmentation potential. The constraints selected were also 13% below and above the standard design parameters values.

2. METHODOLOGY

The Eulerian-Eulerian TFM-KTGF approach is described in this section, as well as the turbulence model employed for the gas phase and the interfacial forces between the gas and solid phases modeling. A fragmentation potential model is proposed, based on a breakage probability function (Pougatch *et al*., 2010) and a collision frequency model (Zhang *et al*., 2014). The factorial experimental design employed in the parametric sensitivity analysis is described. The proposed methodology for the CFD-Based optimization consists of coupling the commercial CFD code ANSYS® *Fluent*™ with the Box's COMPLEX algorithm (Box, 1965).

2.1. Transport Equations

The mass and momentum conservation equations for the gas and solid phases are obtained by ensemble averaging of the Navier-Stokes equations. A monodisperse approach is employed for the solid phase and heat and mass transfer are neglected.

$$\frac{\partial}{\partial t}\left(\alpha_g \rho_g\right) + \boldsymbol{\nabla}\cdot\left(\alpha_g \rho_g \boldsymbol{v}_g\right) = 0; \qquad \frac{\partial}{\partial t}\left(\alpha_p \rho_p\right) + \boldsymbol{\nabla}\cdot\left(\alpha_p \rho_p \boldsymbol{v}_p\right) = 0 \tag{1a,b}$$

$$\frac{\partial}{\partial t}\left(\alpha_g \rho_g \boldsymbol{v}_g\right) + \boldsymbol{\nabla}\cdot\left(\alpha_g \rho_g \boldsymbol{v}_g \boldsymbol{v}_g\right) = -\alpha_g \boldsymbol{\nabla} P - \boldsymbol{\nabla}\cdot \alpha_g \boldsymbol{T}_g + \alpha_g \rho_g \boldsymbol{g} - \boldsymbol{F}_{gp} \tag{2a}$$

$$\frac{\partial}{\partial t}\left(\alpha_p \rho_p \boldsymbol{v}_p\right) + \boldsymbol{\nabla}\cdot\left(\alpha_p \rho_p \boldsymbol{v}_p \boldsymbol{v}_p\right) = -\alpha_p \boldsymbol{\nabla} P - \boldsymbol{\nabla} P_{p,s} - \boldsymbol{\nabla}\cdot \alpha_p \boldsymbol{T}_p + \alpha_p \rho_p \boldsymbol{g} + \boldsymbol{F}_{gp} \tag{2b}$$

t, α, ρ, $\boldsymbol{v}$, P, $\boldsymbol{T}$, $\boldsymbol{g}$ and $\boldsymbol{F}$ represents the time, volume fraction, density, velocity vector, pressure, effective stress tensor, gravitational field and gas-particle interaction force, respectively. The sub-index g represents the gas phase and the sub-index p the solid phase. $P_{p,s}$ represents the solid phase pressure, described by the KTGF model. The $k-\varepsilon$ turbulence model is employed to resolve the gas phase effective stress tensor, which is written in Eq. (3). The turbulent viscosity $({\mu_g}^t)$ is written as a function of the turbulent kinetic energy (k) and the dissipation rate of turbulent kinetic energy (ε).

$$\boldsymbol{T}_g = \boldsymbol{\tau}_g + {\boldsymbol{\tau}_g}^t = -\left(\mu_g + {\mu_g}^t\right)\left[\boldsymbol{\nabla}\boldsymbol{v}_g + \left(\boldsymbol{\nabla}\boldsymbol{v}_g\right)^T - \frac{2}{3}\boldsymbol{I}\boldsymbol{\nabla}\cdot\boldsymbol{v}_g\right] + \frac{2}{3}\rho_g k\boldsymbol{I}; \qquad {\mu_g}^t = C_\mu \rho_g \frac{k^2}{\varepsilon} \tag{3a,b}$$

μ_g represents the gas phase dynamic viscosity and $C_\mu = 0.09$. The transport equations for the turbulent kinetic energy and the dissipation rate of turbulent kinetic energy are given by:

$$\rho_g\left[\frac{\partial k}{\partial t} + \boldsymbol{\nabla}\cdot\left(\boldsymbol{v}_g k\right)\right] = \boldsymbol{\nabla}\cdot\left[\left(\mu_g + \frac{{\mu_g}^t}{\sigma_k}\right)\boldsymbol{\nabla} k\right] + G_k - \rho_g \varepsilon \tag{5}$$

$$\rho_g\left[\frac{\partial \varepsilon}{\partial t} + \boldsymbol{\nabla}\cdot\left(\boldsymbol{v}_g \varepsilon\right)\right] = \boldsymbol{\nabla}\cdot\left[\left(\mu_g + \frac{{\mu_g}^t}{\sigma_\varepsilon}\right)\boldsymbol{\nabla}\varepsilon\right] + C_{\varepsilon,1}\frac{\varepsilon}{k}G_k - C_{\varepsilon,2}\rho_g\frac{\varepsilon^2}{k} \tag{6}$$

the term G_k related to the production of turbulent kinetic energy, given by Eq. (7). The constants are listed: $\sigma_k = 1.0$, $\sigma_\varepsilon = 1.3$, $C_{\varepsilon,1} = 1.44$ and $C_{\varepsilon,2} = 1.92$.

$$G_k = \left(\mu_g + {\mu_g}^t\right)\left[\boldsymbol{\nabla}\boldsymbol{v}_g + \left(\boldsymbol{\nabla}\boldsymbol{v}_g\right)^T : \boldsymbol{\nabla}\boldsymbol{v}_g\right] \tag{7}$$

The granular temperature (Θ) is used to model the turbulent energy fluctuations for the solid phase considering that the particle movement induced by particle-particle collisions is analogue to the movement of gas molecules promoted by temperature increase (Grace *et al*., 2020). The granular temperature transport equation is written in Eq. (8).

$$\frac{3}{2}\left[\frac{\partial}{\partial t}\left(\rho_p\alpha_p\Theta_p\right)+\boldsymbol{\nabla}\cdot\left(\rho_p\alpha_p\boldsymbol{v}_p\Theta_p\right)\right]=\left(-P_{p,s}\boldsymbol{I}+\boldsymbol{T}_p\right):\boldsymbol{\nabla}\boldsymbol{v}_p+\boldsymbol{\nabla}\cdot\left(k_{\Theta_p}\boldsymbol{\nabla}\Theta_p\right)-\gamma_{\Theta_p}+\phi_{gp} \tag{8}$$

$\boldsymbol{I}$ is the unit tensor, k_{Θ_p} represents the granular temperature diffusive coefficient, γ_{Θ_p} represents the collisional dissipation of granular energy and ϕ_{gp} represents the granular energy production. The solid phase pressure is given by Eq. (9):

$$P_{p,s}=\rho_p\alpha_p\Theta_p\left[1+2\alpha_p g_0\left(1+e_p\right)\right] \tag{9}$$

e_p denotes the particle-particle restitution coefficient and g_0 a radial distribution function, described in this work with the Lun *et al*. (1984) model.

$$g_0=\left[1-\left(\frac{\alpha_p}{\alpha_{p,max}}\right)^{\frac{1}{3}}\right]^{-1} \tag{10}$$

$\alpha_{p,max}=0.63$. The stress tensor for the solid phase is given by Eq. (11):

$$\boldsymbol{T}_p=\mu_p\left[\boldsymbol{\nabla}\boldsymbol{v}_p+\left(\boldsymbol{\nabla}\boldsymbol{v}_p\right)^T\right]+\left(\lambda_p-\frac{2}{3}\mu_p\right)\boldsymbol{I}\cdot\boldsymbol{\nabla}\cdot\boldsymbol{v}_p \tag{11}$$

μ_p is the solid phase shear viscosity and λ_p the solid phase apparent viscosity. The shear viscosity is a function of the collisional viscosity (${\mu_p}^{col}$), the granular viscosity (${\mu_p}^{kin}$) and the friction viscosity (${\mu_p}^{fr}$). The collisional and granular viscosities are given by Syamlal *et al*., (1993) model and the friction viscosity is described by Schaeffer (1987) model.

$$\mu_p={\mu_p}^{col}+{\mu_p}^{kin}+{\mu_p}^{fr};\qquad {\mu_p}^{col}=\frac{4}{5}\rho_p{\alpha_p}^2 d_p g_0\left(1+e_p\right)\sqrt{\frac{\Theta_p}{\pi}} \tag{12a,b}$$

$${\mu_p}^{kin}=\frac{4\rho_p\alpha_p d_p\sqrt{\Theta_p\pi}}{6\left(3-e_p\right)}\left[1+\frac{2}{5}\left(1+e_p\right)\left(3e_p-1\right)\alpha_p g_0\right];\qquad {\mu_p}^{fr}=P_{p,s,fr}\left(\boldsymbol{I}-\frac{sen\left(\phi_p\right)}{\sqrt{I_{2D}}}\boldsymbol{D}_p\right) \tag{12c,d}$$

$P_{p,s,fr}$ represents the frictional pressure, given by Johnson *et al*. (1990) model. ϕ_p is the friction internal angle, equivalent to $\phi_p=30{,}00007°$, $\boldsymbol{D}_p$ is the strain rate tensor and I_{2D} the second invariant of the strain rate tensor.

$$P_{p,s,fr}=\begin{cases}0,\alpha_p<\alpha_{p,t}\\ 0{,}05\frac{\left(\alpha_p-\alpha_{p,t}\right)^2}{\left(\alpha_{p,max}-\alpha_p\right)^5},\ \alpha_p\geq\alpha_{p,t}\end{cases},\ \alpha_{p,t}=0{,}615;\qquad \boldsymbol{D}_p=\frac{1}{2}\left[\boldsymbol{\nabla}\boldsymbol{v}_p+\left(\boldsymbol{\nabla}\boldsymbol{v}_p\right)^T\right] \tag{13a,b}$$

The solid phase apparent viscosity and the collisional dissipation rate of granular temperature are given by Lun *et al*. (1984) models and the granular temperature diffusive coefficient is described by Syamlal *et al*. (1993) model. The production of granular temperature is given by Gidaspow (1994) model. β_{gp} represents the drag coefficient.

$$\lambda_p=\frac{4}{3}\rho_p{\alpha_p}^2 d_p g_0\left(1+e_p\right)\sqrt{\frac{\Theta_p}{\pi}};\qquad \gamma_{\Theta_p}=12\left(1-{e_p}^2\right)\frac{\rho_p{\alpha_p}^2 g_0}{d_p\sqrt{\pi}}{\Theta_p}^{\frac{3}{2}};\qquad \phi_{gp}=-3\beta_{gp}\Theta_p \tag{14a,b,c}$$

$$k_{\Theta_p}=15\frac{\rho_p\alpha_p d_p\sqrt{\Theta_p\pi}}{4\left(41-33\eta\right)}\left[1+\frac{12}{5}\eta^2\left(4\eta-3\right)\alpha_p g_0+\frac{16}{15\pi}\left(41-33\eta\right)\eta\alpha_p g_0\right],\quad \eta=\frac{1}{2}\left(1+e_p\right) \tag{15a,b}$$

2.2. Interfacial Forces

Only the drag force is considered among the interfacial momentum exchange forces between the gas and solid phases. The particle to gas density ration is big enough for the lift, virtual masses, Basset, Saffman and Magnus forces to be negligible (Grace *et al*., 2020).

$$\boldsymbol{F}_{gp,D}=\beta_{gp}\left(\boldsymbol{v}_g-\boldsymbol{v}_p\right) \tag{16}$$

The drag coefficient is given through the Shah *et al*. (2015) *EMMS* model, considering different coefficients according to different volume fractions of the solid phase.

$$\beta_{gp} = \begin{cases} 150\frac{{\alpha_p}^2\mu_g}{\alpha_g {d_p}^2} + 1{,}75\frac{|v_p - v_g|}{d_p}\rho_g\alpha_p, & \alpha_g < 0{,}6 \\ \frac{3}{4}C_{D,gp,D}\frac{|v_p - v_g|}{d_p}\rho_g\alpha_g\alpha_p f(\alpha_x), & x \geq \alpha_x \end{cases} \quad (17)$$

For $0{,}6 \leq \alpha_x \leq 0{,}8$,
$(\alpha_x) = 1449{,}20{\alpha_g}^4 - 4692{,}40{\alpha_g}^3 + 5722{,}40{\alpha_g}^2 - 3117{,}20\alpha_g + 641{,}1$
For $0{,}8 < \alpha_x \leq 0{,}98$,
$f(\alpha_x) = 124{,}77{\alpha_g}^4 - 474{,}59{\alpha_g}^3 + 681{,}97{\alpha_g}^2 - 439{,}94\alpha_g + 108{,}15$ (18)
For For $\alpha_x > 0{,}98$,
$f(\alpha_x) = 30{,}739\alpha_g - 29{,}739$

$C_{D,gp,D}$ is the drag coefficient for an insulated particle, Re_p is the particle Reynolds number and d_p is the particle Sauter diameter.

$$C_{D,gp,D} = \begin{cases} 0{,}44 & , \quad Re_p > 1000 \\ \frac{24}{Re_p}\left[1 + 0{,}15{Re_p}^{0{,}687}\right], & Re_p < 1000 \end{cases} ; \qquad Re_p = \frac{\rho_g\alpha_g|v_g - v_p|d_p}{\mu_g} \quad (19a,b)$$

2.3. Fragmentation Potential Modeling

The fragmentation potential is written based on Pougatch *et al*. (2010) breakage probability function, considering binary particle-particle collisions. This approach considers the particulate material mechanical properties with a breakage constant (C_{br}) in the form of a breakage activation energy, the particle diameter (d_p) and the particle velocity (v_p). The higher the velocity impact, closer to 1.0 is the breakage probability function value. The breakage probability is combined with Zhang *et al*. (2014) collision frequency model, described as a function of the flow field and solid phase properties.

$$F_{pot} = f_{coll}P_{br}; \qquad P_{br} = e^{-\left(\frac{C_{br}}{d_p{v_p}^2}\right)}; \qquad f_{coll} = 8{,}4853\left(1 - \alpha_g\right)\frac{v_p}{d_p} \quad (20a,b,c)$$

A value of $C_{br} = 0.21\ \mathrm{m^3/s^2}$ was estimated for coal particles by Pougatch *et al*. (2010). The particulate material analyzed in the present work is FCC catalyst and no data regarding the breakage constant was found, therefore, a value of $C_{br}/100$ is employed in the present work with the objective of simulating the fragmentation potential a particulate material with a much smaller mechanical resistance than the original coal sample. The fragmentation potential spatial and time averaged value is employed in the analysis performed in this work in order to investigate the influence of different injection nozzle design parameters on the particle breakage. The fragmentation potential value in cell is integrated on the domain volume following Eq. (21a) and the accumulated value in time is calculated through Eq. (21b). The sub-index e represents the computational cell, the sub-index j the evaluated time-step and V the cell volume. To compare the results obtained with each test case, the mean value of F_{pot_j} is calculated by Eq. (21c).

$$\int {F_{pot}}_t dV = \sum_{e=1}^{n_e} {F_{pot}}_{e,t}|V_e| = \sum_{e=1}^{n_e} 8{,}4853\left(1 - {\alpha_g}_{e,t}\right)\frac{{v_p}_{e,t}}{d_p}e^{-\left(\frac{C_{br}}{d_p{v_p}_{e,t}^2}\right)}|V_e| \quad (21a)$$

$$F_{pot_j} = \sum_{t=1}^{n_t}\frac{1}{t_t}\int {F_{pot}}_t dV; \qquad F_{pot,m} = \frac{1}{n_{t,sim}}\sum_{j=1}^{n_{t,sim}} F_{pot_j} \quad (21b,c)$$

2.4. Test Setups

The analyzed dense fluidized bed is based on the LP-ECT unit constructed on the Blumenau Regional University (FURB). The inner diameter and the considered height of the equipment are respectively $D = 100$ mm and $H = 1000$ mm. A scheme of the LP-ECT unit is shown in Fig. 1.a. The inlet nozzle region is amplified and the gas inlet configuration is shown if Fig. 1.b. and the inlet nozzle design parameters are summarized in Fig. 1.c. The particulate material employed in the analysis is equilibrium FCC catalyst with a Sauter mean diameter of $d_p = 65$ μm and a particle density of $\rho_p = 1500\ \mathrm{kg/m^3}$, being classified as a Geldart A type particle. The static bed height considered is $H_b = 400$ mm, which results in a bed mass of $W_b = 3205.21$ g and a bulk bed density of $\rho_b = 1020.25\ \mathrm{kg/m^3}$. Air is injected in the system at ambient temperature and atmospheric pressure at a volumetric flow rate of $\dot{Q}_g = 60\ \mathrm{L/min}$, which results in an orifice inlet velocity of $v_{or} = 33.55\ \mathrm{m/s}$ and a superficial gas velocity of $U = 12.73\ \mathrm{cm/s}$. The original inlet nozzle design parameters are listed in Tab. 1, as well as the values calculated for the parametric sensitivity analysis (PSA), 13% below and above the original values, resulting in a total of 32 numerical experiments (2^5 factorial design). The bed properties

and the gas inlet flow rate are kept constant throughout all test cases performed on the parametric sensitivity analysis and CFD-based optimization.

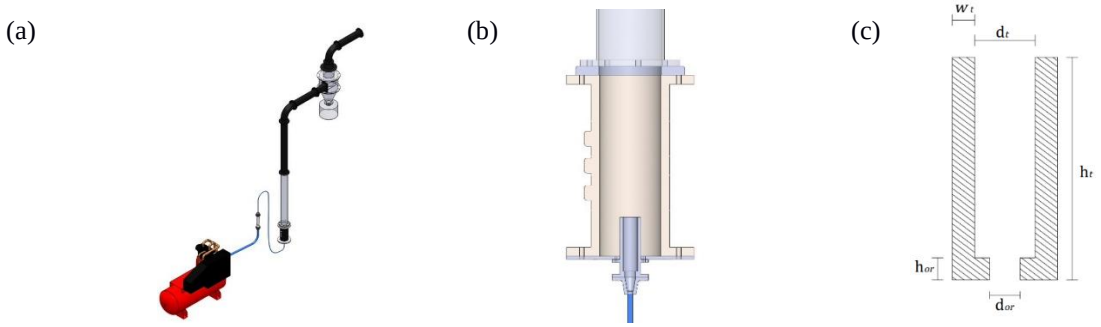

Figure 1. (a) LP-ECT unit scheme. (b) Inlet nozzle region. (c) Inlet nozzle design parameters.

Table 1. Inlet nozzle design parameters – original and employed in the designed numerical experiments for the PSA.

Design Level	d_{or} (mm)	d_t (mm)	h_{or} (mm)	h_t (mm)	w_t (mm)
0	6.1600	8.1800	2.1000	50.0000	1.2500
−	5.3592	7.1166	1.8270	43.5000	1.0875
+	6.9608	9.2434	2.3730	56.5000	1.4125

2.5. Numerical Setup

A 2D-axysimmetric approach is employed on the spatial discretization of the proposed domain through the use of the Finite Volume Method (FVM). The numerical mesh is constructed considering a maximum element size of $l_e = 10d_p$ at the analysis region (the jets region), in order to properly capture the gas-solid interface and therefore represent accurately the studied effect (Andrews *et al*., 2005). The mesh has element sizes of $l_e = 0.2$ mm on the inlet nozzle region, $l_e = 0.75$ mm in the freeboard region and $l_e = 0.2$ mm $- 0.7$ mm in the jet's region, as shown in Fig. 2.

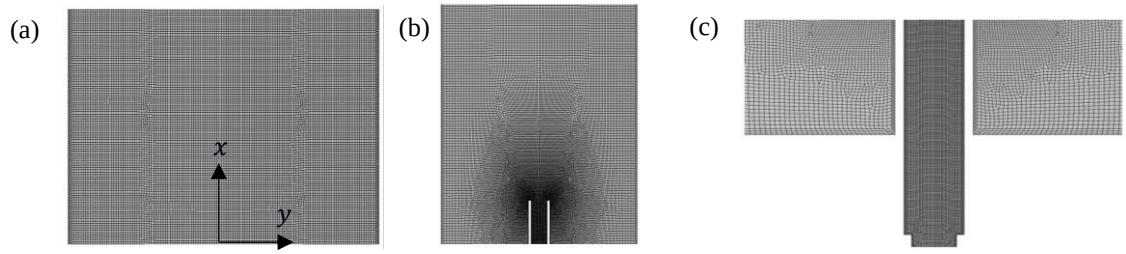

Figure 2. Numerical mesh at different regions (a) Freeboard. (b) Jet's region. (c) Inlet nozzle.

The Phase-Coupled SIMPLE algorithm is employed on the numerical model solution (Patankar and Spalding, 1972; Vasquez and Ivanov, 2000). The boundary conditions considered are: gas inlet mass flow of $\dot{W}_g = 1{,}25 \times 10^{-3}$ kg/s, pressure outlet on the top of the equipment, no-slip wall for the gas phase and a specularity coefficient of $\emptyset_{p,s} = 0{,}1$, a particle-wall restitution coefficient of $e_w = 0{,}6$ for and a particle-particle restitution coefficient of $e_p = 0{,}99$ for the solid phase (Chalermsinsuwan *et al*., 2012; Loha *et al*., 2013; Loha *et al*., 2014). A symmetry condition is employed in the height of the equipment, starting from $y = 0$ and the time-step used was $\Delta t = 2 \times 10^{-5}$ s.

2.6. Parametric Sensitivity Analysis

As described in Tab. 1, 32 different inlet nozzle configurations are analyzed on the PSA. A total flowtime of 7 s is calculated for each test, with all the numerical experiments starting from the same initial condition, consisting of 10 s flowtime for the original inlet nozzle configuration. The first 2 s are not considered on the results evaluation. Several jet cycles occurred during the evaluated flowtime. The software STATISTICA® 8.0 is used on the data analysis, with a confidence interval of 95%. The mean value of the accumulated fragmentation potential is used on the comparison, calculated through Eq. (20c). The p-value is calculated and the design variables of the inlet nozzle that have a significant influence on the fragmentation potential are obtained.

2.7. CFD-Based Optimization

The significant inlet nozzle design variables found on the PSA are used as geometric restrictions on the COMPLEX algorithm (Box, 1965) and the mean value of the accumulated fragmentation potential is used as an objective function to be minimized. The algorithm is described in details in the work of Sgrott Jr *et al*. (2015). The objective function and the lower and upper restrictions employed are described below for a generic case on which all of the design variables are significant.

$$\text{Minimize} \quad F_{pot,m}(d_{or}, d_t, h_{or}, h_t, w_t),$$
$$\text{restrictions} \begin{cases} d_{or,low} < d_{or} < d_{or,up} \\ d_{t,low} < d_t < d_{t,up} \\ h_{or,low} < h_{or} < h_{or,up} \\ h_{t,low} < h_t < h_{t,up} \\ w_{t,low} < w_t < w_{t,up} \end{cases}. \tag{21}$$

The geometrical restriction values employed on the optimization procedure are the same as the ones employed on the PSA, except for the non-significant variables, on which the standard value is considered. A total flowtime of 1.5 s is considered on this analysis, with every analyzed case starting from the same initial condition, the same employed on the PSA. The optimization procedure is described on Fig. 3. The initial SIMPLEX is composed by the standard test, the tests that obtained the worst and best results for the fragmentation potential (higher and lower) and two random cases. The index K represents the iteration.

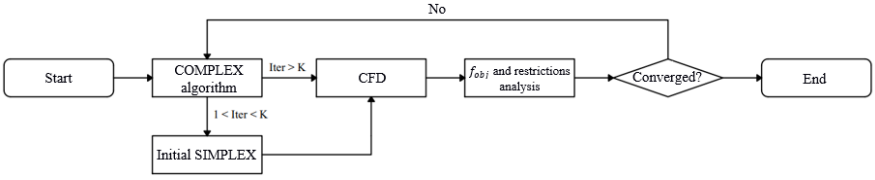

Figure 3. CFD-Based optimization solution procedure.

The convergence criteria/tolerance used is the absolute error between the previous $(z-1)$ and the current iteration (z) obtained results for $F_{pot,m}$. A value of $Tol < 1.0 \times 10^{-3}$ is employed.

$$Tol = \ 1 \times 10^{5} \left| F_{pot,m_z} - F_{pot,m_{z-1}} \right| \tag{22}$$

3. RESULTS AND DISCUSSION

The results obtained in the PSA and CFD-Based Optimization are presented in this section. The significant variables obtained in the statistical analysis developed in the PSA are employed as geometrical restrictions on the optimization.

3.1. Parametric Sensitivity Analysis Results

Firstly, the $F_{pot,m}$ values obtained for the 32 analyzed inlet nozzle geometries are presented in Fig. 4.a. The red dashed line indicates the result obtained for the standard test case. The test cases with the upper and lower limits for both orifice diameter and tube diameter obtained results on the same order of magnitude - ${d_{or}}^{+}, {d_t}^{+}$ and ${d_{or}}^{-}, {d_t}^{-}$, tests 1-8 and 25-32, respectively. Tests 9-16 resulted on higher values for the analyzed variable, showing that the combination ${d_{or}}^{+}, {d_t}^{-}$ is not suitable when the minimization of the fragmentation potential is desired. On the other hand, tests 17-24 showed smaller values for the studied variable, therefore, the combination ${d_{or}}^{-}, {d_t}^{+}$ is interesting. The inlet nozzle geometry for the tests that obtained the worst and best results regarding the mean value of the fragmentation potential are drawn in Fig. 4.b. Test 15 showed the worst result, with $F_{pot,m} = 3{,}6 \times 10^{-3}$, while test 19 showed the best result, with $F_{pot,m} = 5{,}68 \times 10^{-6}$. The mean fragmentation potential value obtained by test 15 is aproximately 633 times bigger than the value obtained with test 19. This difference is mainly related with the gas velocity at the the inlet nozzle exit, highly influenced by the presence of the orifice, with values of $v_t = 26.3$ m/s for test 15 and $v_t = 18.1$ m/s for test 19.

The influence of the nozzle design parameters is statistically analyzed with the p-value test. Fig. 5 summarizes the pareto chart considering three-way interactions between the variables employed on the analysis, with an 95% confidence interval, obtained with the software STATISTICA® 8.0. The obtained coefficient of determination has a value of $R^2 = 0.9910$.

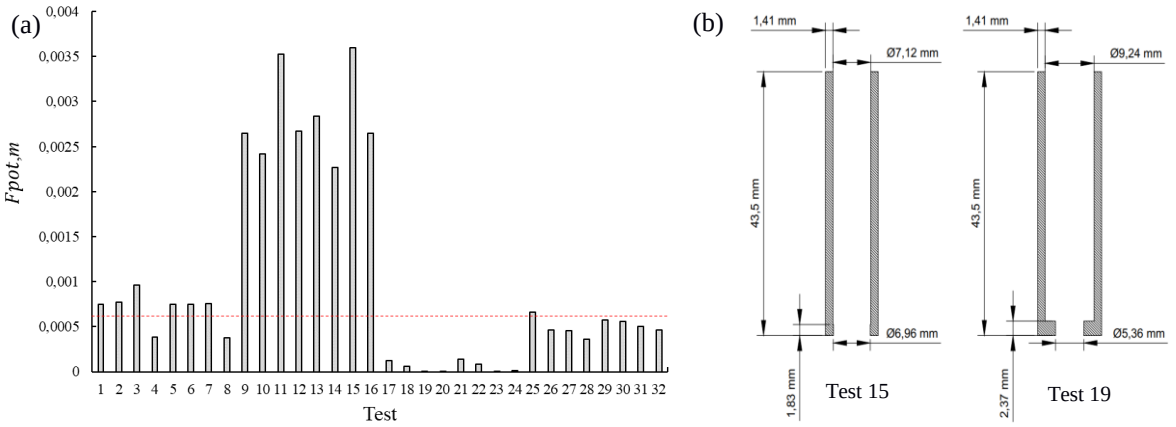

Figure 4. PSA test cases results comparison. (a) All tests comparison. (b) Worst and best results obtained.

As expected from the results analyzed in Fig. 4.a, the orifice diameter and the tube diameter have the most influence on the fragmentation potential. The tube height (h_t) and tube wall thickness (w_t) also have a significative influence on the analyzed effect, with $p < 0.05$. The only variable with no significant influence, according to the p-value test, is the orifice height (h_{or}). The significant inlet nozzle design parameters d_{or}, d_t, h_t and w_t are then employed as geometrical restrictions and variables to be optimized on the CFD-Based Optimization procedure.

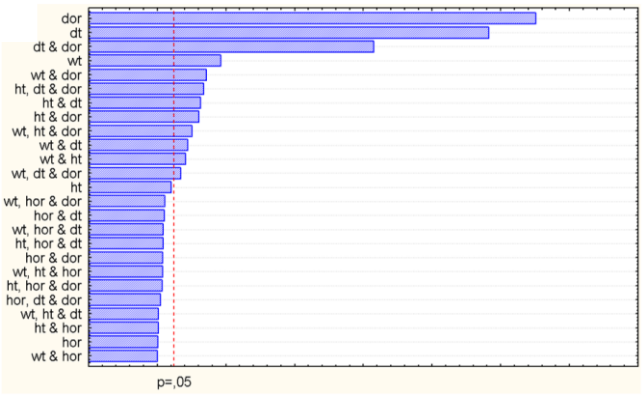

Figure 5. Pareto chart obtained.

3.2. CFD-Based Optimization Results

As mentioned before, the significant variables obtained through the PSA are employed as geometrical restrictions on the optimization procedure. The lower and upper limits are considered the same values employed on the PSA analysis, described in Tab. 1, except for the variable h_{or}. The initial SIMPLEX is composed by 5 points: the test cases that obtained the worst and best results for $F_{pot,m}$, 15^* and 19^*, respectively; the test cases on which all the variables have the upper limit value and the lower limit value, 1^* and 32^*, respectively; and the standard test case. The COMPLEX algorithm is fed with a wide range of results for the objective function and therefore a fast convergence is expected. Fig. 6a. shows the objective function evolution for 25 COMPLEX algorithm iterations.

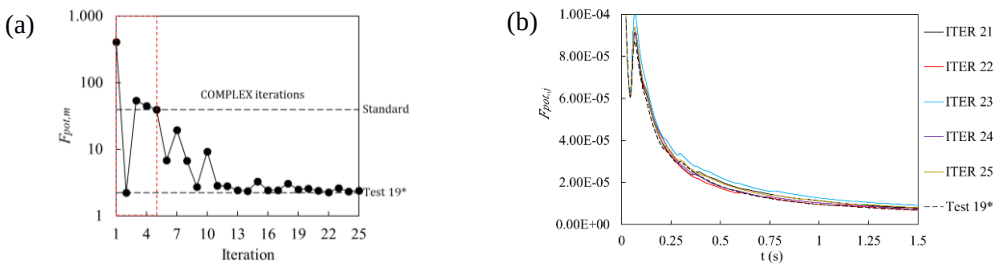

Figure 6. (a) Objective function evolution. (b) 5 last COMPLEX algorithm results compared to test 19^*.

The dashed red line represents the 5 points of the initial SIMPLEX, on which big variations between the $F_{pot,m}$ values are observed. For the analyzed results, test 19^* showed the smaller value for the objective function and it is expected that the optimized inlet nozzle design parameters will approach this test case values. The behavior of the cumulated value of the fragmentation potential for the last 5 COMPLEX algorithm iterations is shown in Fig. 6b, comparing them with test 19^*.

Fig. 7. shows the evolution of the manipulated variables according to the COMPLEX algorithm iteration. The lower and upper limits are presented as dashed lines, as well as the standard test case value. The orifice diameter tends to reach a value close to the lower limit imposed and the tube diameter is almost immediately locked at the upper limit value. The tube height tends to reach a value equivalent to the lower limit, while the tube wall thickness stays in between the values of the upper limit and the standard case. The values observed up until the present iteration are close to test 19^* parameters, except for the tube wall thickness. The tendency observed is that lower velocities at the inlet nozzle exit results in lower $F_{pot,m}$ values.

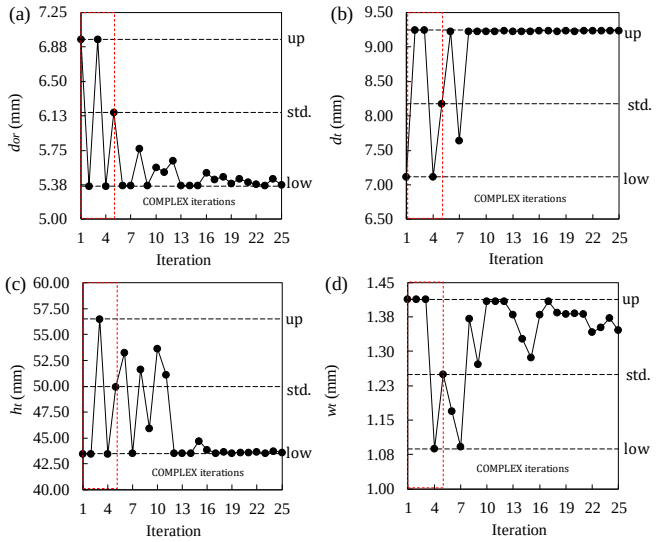

Figure 7. Manipulated variables evolution. (a) d_{or}. (b) d_t. (c) h_t. (d) w_t.

4. CONCLUSIONS

The proposed TFM-KTGF based fragmentation potential model is sensible to variations on the inlet nozzle design parameters and the flowtimes simulated were sufficient to account for the effect of multiple jet cycles even when short times were considered (1.5 s). On the PSA, high sensibility of the fragmentation potential to the orifice and tube diameters was observed, being this mainly related to the nozzle outlet velocity. The difference between the worst (test 15) and best (test 19) results was of 633 times. All inlet nozzle design parameters have significant influence over the fragmentation potential, except for the orifice height, as shown in the PSA statistical analysis through the p-value test. The initial SIMPLEX proposed for the CFD-Based Optimization procedure helped at the COMPLEX algorithm convergence, however, for the analyzed iterations (25), the tolerance was not achieved. The best result obtained for the fragmentation potential on the optimization procedure is for the test 19^* and the results from the last 5 iterations show a tendency for the manipulated variables to meet test's 19^* values, except for the tube wall thickness, that's currently found in between the standard test and the upper limit values.

5. ACKNOWLEDGEMENTS

The authors would like to thank PETROBRAS and FUNCAMP for the funding provided for the work development.

6. REFERENCES

Box, M. J., 1965. "A new method of constrained optimization and a comparison with other methods". *The Computer Journal*, Vol. 8 (1), p. 42-52.

Chalermsinsuwan, B., Gidaspow, D., Piumsomboon, P., 2011. "Two- and three-dimensional CFD modeling of Geldart A particles in a thin bubbling fluidized bed: Comparison of turbulence and dispersion coefficients". *Chemical Engineering Science*, Vol. 171, p. 301-303.

Fulchini, F., Nan, W., Ghadiri, M., Yazdan panah, M., Bertholin, S., Amblard, B., Cloupet, A., gauthuier, T., 2017. "CFD-DEM Analysis of Particle Attrition in a Jet in a Fluidized Bed". *8th International Conference of Micromechanics on Granular Media, Powers and Grains 2017*, Vol. 140, p. 03-07.

Geldart, D., 1973. "Types of gas fluidization". *Powder Technology*, Vol. 7 (5), p. 285-292.

Ghadiri, M., Zhang, Z., 2002. "Impact attrition of particulate solids. Part 1: Theoretical model". *Chemical Engineering Science*, Vol. 57, p. 3659– 3669.

Ghods, N., Golshan, S., Zarghami, R., sotudeh-gharebagh, R., 2019. "CFD-DEM modelling of particles attrition in jet-in-fluidized beds". *Chemical Engineering Research and Design*, Vol. 148, p. 336-348.

Gidaspow, D., 1994. *Multiphase flow and fluidization*. Academic Press, Boston.

Grace, J. R., Bi, X., Ellis, N., 2020. *Essentials of fluidization technology*. Wiley-VHC Verlag GmbH & Co. KGaA.

Hoef, M. A. van der., Annaland, M. van Sint., Deen, N. G., Kuipers, J. A. M., 2008. "Numerical simulation of dense gas-solid fluidized beds: a multiscale modeling strategy". *Annual Review of Fluid Mechanics*, Vol. 40, p. 47-70.

Johnson, P. C., Jackson, R., 1987. "Frictional-collisional constitutive relations for granular materials, with application to plane shearing". *Journal of Fluid Mechanics*, Vol. 176, p. 67-93.

Kang, P., Hu, X. E., Lu, Y., Wang, K., Zhang, R., Han, L., Yuan, H., Chen, H., Luo, X., Zhou, Y. J., 2020. "Modeling and optimization for gas distribution patterns on biomass gasification of a bubbling spout fluidized bed". *American Chemical Society*, Vol. 34 (2), p. 1750-1763.

Lim, K. S., Zhu, J. X., Grace, J. R., 1995. "Hydrodynamics of gas-solid fluidization". *International Journal of Multiphase Flow*, Vol. 21, p. 141-193.

Loha, C., Chattopadhay, H., Chatterjee, P. K., 2013. "Euler-Euler CFD modeling of fluidized bed: Influence of specularity coefficient on hydrodynamic behavior". *Particuology*, Vol. 11 (6), p. 673-680.

Loha, C., Chattopadhay, H., Chatterjee, P. K., 2014. "Effect of coefficient of restitution in Euler-Euler CFD simulation of fluidized-bed hydrodynamics". *Particuology*, Vol. 15, p. 170-177.

Luciano, R. D., Silva, B. L., Rosa, L. M., Meier, H. F., 2018. "Multi-objective optimization of cyclone separators in series based on computational fluid dynamics". *Powder Technology*, Vol. 325, p. 452-466.

Lun, C. K. K., Savage, S. B., Jeffrey, D. J., Chepuriny, N., 1984. "Kinetic theories for granular flow: inelastic particles in Couette flow and slightly inelastic particles in a general flowfield". *Journal of Fluid Mechanics*, Vol. 140, p. 223-257.

McMillan, J., Briens, C., Berutti, F., Chan, E., 2007. "Particle attrition mechanism with a sonic gas jet injected into a fluidized bed". *Chemical Engineering Science*, Vol. 62, p. 3809-3820.

Nelder, J. A., Mead, R. A., 1965. "A SIMPLEX method for function minimization". *The Computer Journal*, Vol. 7 (4), p. 308-313.

Pougatch, K., Salcudean, M., McMillan, J., 2010. "Simulation of particle attrition by supersonic gas jets in fluidized beds". *Chemical Engineering Science*, Vol. 65 (16), p. 4829-4843.

Powell, M. J. D., 2007. "A view of algorithms for optimization without derivatives". *Mathematics Today*, Vol. 43 (5), p. 170-174.

Sadeghbeigi, R., 2020. *Fluid catalytic cracking handbook: design, operation and troubleshooting of FCC facilities*. Gulf Professional Publishing, Houston, 2nd edition.

Sauriol, P., Cui, H., Cahouki, J., 2013. "Gas jet penetration lengths from upward and downward nozzles in a dense gas-solid fluidized bed". *Powder Technology*, Vol. 235, p. 42-54.

Schaeffer, D. G., 1987. "Instability in the evolution equations describing incompressible granular flow". *Journal of Differential Equations*, Vol. 66 (1), p. 19-50.

Sgrott Jr, O. L., Noriler, D., Wiggers, V. R., Meier, H. F., 2015. "Cyclone optimization by COMPLEX method and CFD simulation". *Powder Technology*, Vol. 277, p. 11-21.

Shah, S., Myöhänen, K., Kallio, S., Hyppänen, T., 2015. "CFD simulations of gas-solid flow in an industrial-scale circulating fluidized bed furnace using subgrid-scale drag models". *Particuology*, Vol. 18, p. 66-75.

Syamlal, M., Rogers, W., O'Brien, T., 1993. *MFIX Documentation: Theory guide*. U.S. Department of Energy.

Vaux, W. G., Keairns, D.L., 1980. *Particle attrition in fluid-bed processes*. In: Grace, J. R., Matsen, J. M., Fluidization, Springer, Boston.

Wu, F., Bai, J., Zhang, J., Zhou, W., Ma, X., 2019. "CFD simulation and optimization of mixing behaviors in a spouted bed with a longitudinal vortex". *American Chemical Society*, Vol. 4 (5), p. 8214-8221.

Yang, W. C., 2003. *Handbook of Fluidization and Fluid-Particle Systems*. Taylor & Francis Inc., New York.

Zhang, B., Zhao, Y., Duan, C., Tang, L., Dong, L., Qu, J., 2014. "Magnetite particle surface attrition model in dense phase gas-solid fluidized bed for dry coal beneficiation". *Advanced Powder Technology*, Vol. 25 (3), p. 1031-1037.

Zhang, H., Degrève, J., Baeyens, J., Wu, S. Y., 2016. "Powder attrition in gas fluidized beds". *Powder Technology*, Vol. 287, p. 1-11.

7. RESPONSIBILITY NOTICE

The authors are the only responsible for the printed material included in this paper.